MATERIALS SCIENCE

Rewritable color nanoprints in antimony trisulfide films

Hailong Liu[1], Weiling Dong[1], Hao Wang[1], Li Lu[1], Qifeng Ruan[1], You Sin Tan[1], Robert E. Simpson[1]*, Joel K. W. Yang[1,2]*

Materials that exhibit large and rapid switching of their optical properties in the visible spectrum hold the key to color-changing devices. Antimony trisulfide (Sb_2S_3) is a chalcogenide material that exhibits large refractive index changes of ~1 between crystalline and amorphous states. However, little is known about its ability to endure multiple switching cycles, its capacity for recording high-resolution patterns, nor the optical properties of the crystallized state. Unexpectedly, we show that crystalline Sb_2S_3 films that are just 20 nm thick can produce substantial birefringent phase retardation. We also report a high-speed rewritable patterning approach at subdiffraction resolutions (>40,000 dpi) using 780-nm femtosecond laser pulses. Partial reamorphization is demonstrated and then used to write and erase multiple microscale color images with a wide range of colors over a ~120-nm band in the visible spectrum. These solid-state, rapid-switching, and ultrahigh-resolution color-changing devices could find applications in nonvolatile ultrathin displays.

INTRODUCTION

Structural colors are unique alternatives to pigments and dyes because a gamut of color can be generated in a wide range of materials by tuning the nanostructure geometry. Structural colors are used to produce two-dimensional (2D) and 3D prints at ultrahigh resolutions (*1*–*3*) by tailoring photonic resonances using advanced nanofabrication techniques. Examples of materials used in structural colors include metals supporting plasmonic resonances (*4*, *5*), dielectrics in nanoantennas (*6*) and photonic crystals (*7*), and magnetic nanoparticles (*8*). Of particular interest are subwavelength thin films of optically lossy materials on metals whose colors are sensitive to the thickness and optical properties of these films alone (*9*, *10*). Chalcogenide phase-change materials (PCMs) (*11*–*14*) can achieve reversible color switching in these systems using an ultrathin form factor. With reversible subnanosecond structural phase transitions causing large changes in their optical constants, PCMs offer fast and stable color changes between amorphous and crystalline states. Moreover, the switching can be repeated billions of times without damaging the materials (*15*–*17*). However, most PCMs, including the widely used $Ge_2Sb_2Te_5$ (GST), exhibit only small refractive index changes and correspondingly small spectral shift of ~35 nm in the visible spectrum when switched between states (*12*–*14*). In contrast, wide-bandgap PCMs, such as antimony trisulfide (Sb_2S_3), provide larger refractive index changes in the visible spectrum (*18*) and are, therefore, desirable for color-changing devices.

Recent efforts to achieve structural color switching (*19*) have relied broadly on refractive index tuning via liquid crystals (*20*) or electrowetting solvents (*21*); mechanical actuation via applied external magnetic fields (*22*) or stretching (*23*); and redox reactions in materials via hydrogenation of metals (*24*, *25*), electrochromic polymers (*26*), and individual molecules (*27*). While electrical approaches to switch colors are arguably the most practical for display applications (*25*), laser writing could induce faster switching and/or be used in situations where electronic control is impossible. Although laser writing has been effective in inducing physical morphological changes in nanostructures to produce color change (*1*, *28*–*30*), these processes are irreversible and do not allow for repeated switching of colors. Recently, we introduced antimony trisulfide (Sb_2S_3) as a wide-bandgap PCM for active visible photonics (*18*). When the phase of Sb_2S_3 is switched, rapid color changes arise from changes in its optical constants. It thus remains interesting to systematically investigate (i) the feasibility of repeated switching, (ii) the gamut and degree of color change as a function of laser power and PCM thickness, and (iii) the smallest pixel size that still exhibits the color switching, which determines the information density and print resolution.

Here, we report a super-high-resolution rewritable color printing method based on reamorphizing Sb_2S_3 with 100-fs duration and 780-nm wavelength laser pulses that are focused to diffraction-limited spots in a nanoscale 3D printer by Nanoscribe GmbH. We explain the subdiffraction measurements with a thermo-optical model. We report the presence of birefringence patterns in crystalline Sb_2S_3 films that were not previously observed and measured the constituent optical constants. We modified the original Sb_2S_3 absorber design (*18*) by removing the top Al film, which would otherwise experience laser-induced damage, thus allowing optical power to be delivered directly to the Sb_2S_3 layer. The result is a color-changing device that can be repeatedly switched.

We used Sb_2S_3 as thin as 10 nm on an Al/Si substrate, with 5-nm Si_3N_4 diffusion barrier layers sandwiching Sb_2S_3. We observed intermediate partially crystalline states that were realized by tuning the energy of the femtosecond laser pulses. Using the large 120-nm shift in the reflectance spectra for these states, multicolor microscale images were printed over the same area of the Sb_2S_3 film. Although the Abbe diffraction limit for the laser writing process was determined to be 780 nm $\left(\frac{\lambda}{2\mathrm{NA}} = \frac{780\ \mathrm{nm}}{2(0.5)}\right)$, we successfully patterned color dots and lines with periodicities down to 600 nm, demonstrating superresolution laser writing. With new measured data of the optical constants, photothermic effects were calculated to rationalize this subdiffraction printing resolution. These color-changing devices and materials characterization are the first steps toward the next generation of displays or inkless erasable papers and could enable camouflaging surfaces, signaling, and compact systems to manipulate the spectral properties of light.

[1]Singapore University of Technology and Design, 8 Somapah Road, Singapore 487372, Singapore. [2]Institute of Materials Research and Engineering (IMRE), 2 Fusionopolis Way, Innovis, #08-03, Singapore 138634, Singapore.
*Corresponding author. Email: robert_simpson@sutd.edu.sg (R.E.S.); joel_yang@sutd.edu.sg (J.K.W.Y.)

RESULTS

Amorphous, crystalline, and intermediate states of Sb_2S_3

Figure 1A shows a schematic of our rewritable color device that consists of thin films of Si_3N_4 (5 nm)/PCM (t nm Sb_2S_3)/Si_3N_4 (5 nm)/Al (100 nm) on a Si substrate. The two layers of Si_3N_4 serve as protection layers and diffusion barriers for the sandwiched chalcogenide PCM (see fig. S1). In contrast to our previous report (*18*), the Al top coating was removed to allow the laser direct access to the PCM (Sb_2S_3) layer. Optical attenuation within the device layers is due to the nontrivial interface reflective phase shifts that lead to resonant absorption (*9*). Accordingly, the proposed rewritable device exhibits resonances, observable as dips (valleys) in the reflectance spectra, and these produce different colors in the reflected light. The resonant wavelengths are dependent on the optical constants and the thickness (t) of the sandwiched PCM. On account of the large refractive index differences between amorphous (A-PCM) and crystalline (C-PCM) states of Sb_2S_3, distinct reversible color changes can be achieved by switching the phase between the A-PCM and C-PCM states.

In contrast to transition metal oxide PCMs, e.g., vanadium dioxide VO_2, which require a constant input of energy to maintain a structural state (*31*), the A-PCM and C-PCM states of Sb_2S_3 are stable at room temperature. In general, crystallization is achieved by elevating the temperature of the material substantially above its glass transition temperature long enough to induce crystal formation. Heating is typically achieved using optical or electrical pulses that are tens of nanoseconds in duration or by heating the entire sample up. Conversely, the crystalline-to-amorphous transition (reamorphization) is induced using high-intensity pulses with short duration to randomize the atomic arrangement, followed by rapid cooling to prevent recrystallizing the material.

In this work, we used 780-nm wavelength femtosecond laser pulses to reamorphize Sb_2S_3, as schematically shown in Fig. 1. By precisely controlling the position and intensity/power of these pulses, we printed a microscale color image at ~40,000-dpi (dots per inch) resolution in the form of Vincent van Gogh's self-portrait, an optical micrograph of which is shown in Fig. 1B. The printed image can be erased by switching the amorphized regions back to the crystalline state. In principle, one can erase selected areas of the prints using a second laser pulse that is longer in duration. However, in our demonstrations, we heated the entire sample on a hot plate to induce crystallization, which erases all the image pixels in parallel and "resets" the sample. Therefore, we could repeatedly write and erase multiple images onto the same region of the device to realize a substrate that enables multiple color prints to be displayed and erased.

To demonstrate color switchability with phase transitions, we start with a 20-nm-thick layer of Sb_2S_3 on 100 nm of Al, as shown in Fig. 2A. The bright-field optical micrographs of the device in the amorphous and crystalline states are shown in Fig. 2A (i and ii, respectively). The device in its amorphous state (i) was imaged as-deposited, and the crystalline sample (ii) was imaged after baking the sample on a hot plate at 300°C for 2 min. The color of the device changes from yellow/orange (amorphous) to purple/blue (crystalline). The blue and purple colors of the crystalline film are attributed to the birefringence of the crystal grains, as discussed in detail later.

Figure 2B shows the measured reflectance spectra of the sample for both states (Fig. 2A, i and ii). The reflectance dip red-shifted by ~120 nm accompanied by an increased full width at half maximum (FWHM) as Sb_2S_3 switched from amorphous to crystalline. The increased FWHM is due to averaging of the two different crystalline colors (purple and blue), and the red shift is caused by the increased refractive index accompanying the amorphous-to-crystalline phase transition (see Fig. 3). The resonance shift (~120 nm) induced by phase transition is much larger than that of the reported GST structures (~35 nm) in the visible region (*12*, *13*). Therefore, our device with Sb_2S_3 has a more pronounced color change compared to that of GST.

Evidence of the amorphous-to-crystalline phase transition in Sb_2S_3 can be seen in the Raman spectra in Fig. 2C. The spectrum of the amorphous sample exhibits two broad bands at ~290 and ~100 cm^{-1}. These bands correspond to the vibrational Sb—Sb bonds in the S_2Sb-SbS_2 structural units and SbS_3 pyramids, respectively (*32*, *33*). For the annealed sample shown in Fig. 2A (ii), the band at 290 cm^{-1} is split into two sub-bands, and the band at ~100 cm^{-1} is further split into many small peaks, consistent with the reported Raman features in crystalline Sb_2S_3 films. These Raman spectra in Fig. 2C confirm that the observed color change in Fig. 2A (i and ii) is driven by the Sb_2S_3 amorphous-to-crystalline phase transition.

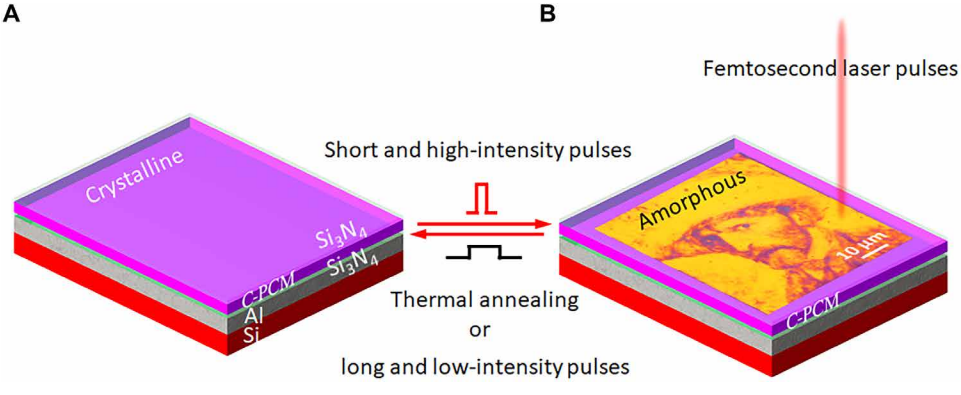

Fig. 1. Rewritable thin-film device. Schematic of the proposed rewritable device consisting of antimony trisulfide PCM switched between (**A**) crystalline (C-PCM) and (**B**) amorphous (A-PCM) states. The thin film consists of Si_3N_4 (5 nm)/Sb_2S_3 (t nm)/Si_3N_4 (5 nm)/Al (100 nm). The reflected colors of the sample are determined by the thickness (t) and the state of the PCM. With t = 20 nm here, the crystalline sample (purple) is amorphized using femtosecond laser pulses (high-intensity pulses with short duration) using a Nanoscribe GmbH two-photon lithography (TPL) system, while the amorphous sample (yellow) is crystallized using a thermal annealing process (effectively similar to providing low-intensity pulses with long duration). Optical micrograph of Vincent van Gogh's self-portrait demonstrating that intermediate states (neither yellow nor purple) can be written on the device by varying exposure power of femtosecond laser pulses and erased via thermal annealing.10 μm

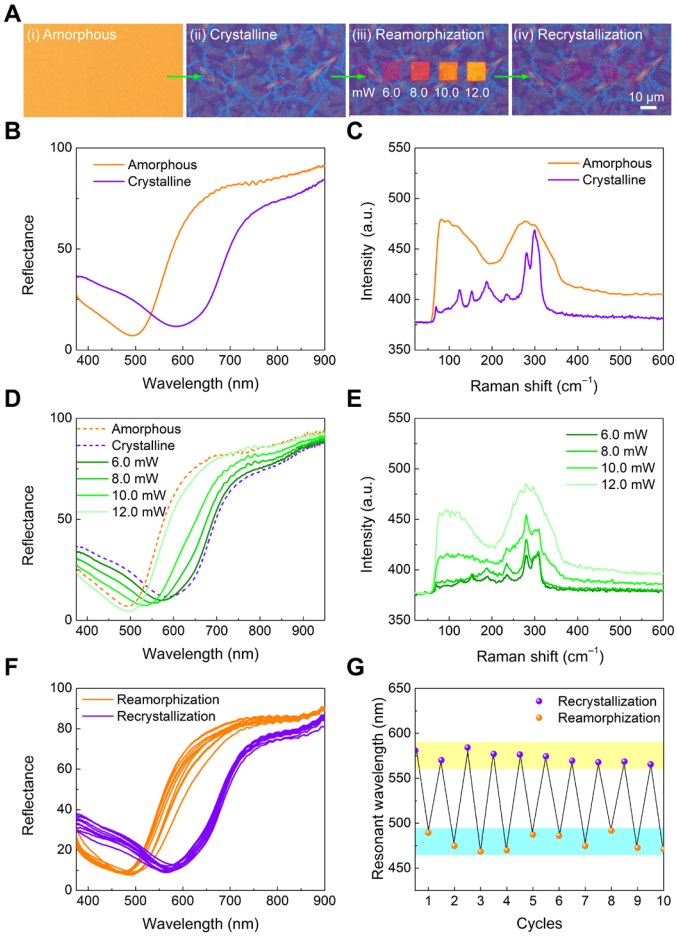

Fig. 2. Phase transitions of Sb_2S_3. (**A**) Optical micrographs of the device with 20-nm-thick Sb_2S_3 in amorphous (i) and crystalline (ii) states. (iii) The crystalline sample can be reamorphized to varying degrees to its original orange color in square areas exposed with increasing excitation power of femtosecond laser pulses from 6.0 to 12.0 mW. (iv) The reamorphized color patches were switched back to the crystalline state after the thermal annealing process. Reflectance (**B** and **D**) and Raman (**C** and **E**) spectra of the amorphous sample, the crystalline sample, and the reamorphized color patches. (**F**) Cyclability measurement for the device with 20-nm-thick Sb_2S_3. (**G**) Reflectance resonant wavelength (valley) as a function of switching cycles. a.u., arbitrary units.

To investigate the switchable and color-tunable properties, we reamorphized the crystalline device in Fig. 2A (ii) using femtosecond laser pulses in the Photonic Professional GT nanoscale 3D printing system by Nanoscribe GmbH. The parameters of our femtosecond laser pulses are as follows: 780-nm wavelength, 80-MHz repetition rate, and 100-fs pulse width (more details in Materials and Methods). The laser beam was raster-scanned over the sample to form 10-μm square color patches. The scan speed was 20 μm/s, and the line step was 400 nm to ensure overlap between the written lines. Figure 2A (iii) shows square patches that were reamorphized under different laser excitation powers. With increasing laser power from 6.0 to 12.0 mW, the blue/purple colors of the crystalline sample increasingly reverted to its orange (amorphous) color. In addition to purely crystalline and amorphous colors, red-purple, red, and red-orange intermediate colors were observed in the transition.

To characterize the states of these color patches, we measured their reflectance and Raman spectra, as shown in Fig. 2 (D and E). The reflectance spectra of the amorphous and crystalline samples are also plotted in Fig. 2D for reference (dashed lines). Notably, the reflectance dips are blue-shifted in a continuous manner as the average laser power was increased from 6.0 to 12.0 mW. Figure 2E shows the Raman spectra of the color patches in Fig. 2A (iii). The Raman features for 6.0 and 8.0 mW are closer to that of the crystalline state, while the characteristics of the Raman spectrum under 10.0 mW match those of the amorphous state. The Raman spectrum of the color patch at 12.0 mW indicates that Sb_2S_3 had completely switched to its amorphous state. Therefore, the thermally crystallized Sb_2S_3 patches were partially reamorphized by the laser power set between 6.0 and 10.0 mW, and it is totally reamorphized at a laser power of 12.0 mW. On the basis of the reflectance and Raman spectra, the color patches of 6.0 to 10.0 mW are intermediate states, i.e., part crystalline and part amorphous. The colors of these patches are linear combinations of the crystalline/amorphous components. Laser powers higher than 20.0 mW caused material ablation and damage (see fig. S2).

A final test of rewritability was performed to carefully determine whether these orange color patches were actually amorphous states of Sb_2S_3 or damaged states. By thermally annealing the sample shown in Fig. 2A (iii) at 300°C for 2 min on a hot plate, we found that the colors could be switched back to that of the crystalline state. This reversal is clearly seen in the optical micrograph of the annealed sample in Fig. 2A (iv), which shows that the partially and completely reamorphized color patches fade to match the color of the surrounding crystalline state. The orientation and sizes of the crystalline domains were preserved during the rewriting process, pointing to further investigation beyond the scope of this communication.

The write-erase cyclability of the color change is important for technological applications. Our tests show that the material can be crystalized and amorphized repeatedly. The reflectance spectra in the amorphous and crystalline states are shown in Fig. 2F, while Fig. 2G shows the resonant wavelength positions as a function of cycling times. Notably, the resonance position and reflectance intensity of the device do not show any deterioration after 10 cycles, despite a spread in the resonance positions, which we ascribe to variations in the exposure conditions between runs, the anisotropic property/birefringence of Sb_2S_3 crystals, the small variation of the crystalline thickness for each crystallization process, and variations in the measurement positions. To the best of our knowledge, this is the first report on reversible color switching that realizes intermediate states for Sb_2S_3 and reveals birefringence within Sb_2S_3 crystal domains. Further endurance tests beyond 10 could be conducted in a setup that writes and rewrites without unmounting the sample, e.g., using electrical probing or multiple laser sources, but is beyond the scope of the current work.

The optical constants were measured and subsequently used to simulate the reflectance and color of the rewritable devices. We measured the refractive index of the 20-nm-thick Sb_2S_3 film within the layer structure shown in Fig. 2A using a micro-ellipsometer by Accurion GmbH equipped with Mueller matrix (see Materials and Methods for details). Figure 3 (A and B) shows the measured real (n) and imaginary (k) components of the refractive index for Sb_2S_3 in the amorphous and crystalline states. These optical constants were measured in the wavelength range of 400 to 900 nm. As the Sb_2S_3 crystalline grain sizes appear to be quite large and considering their orthorhombic crystal structure, in-plane anisotropy [see Fig. 2A

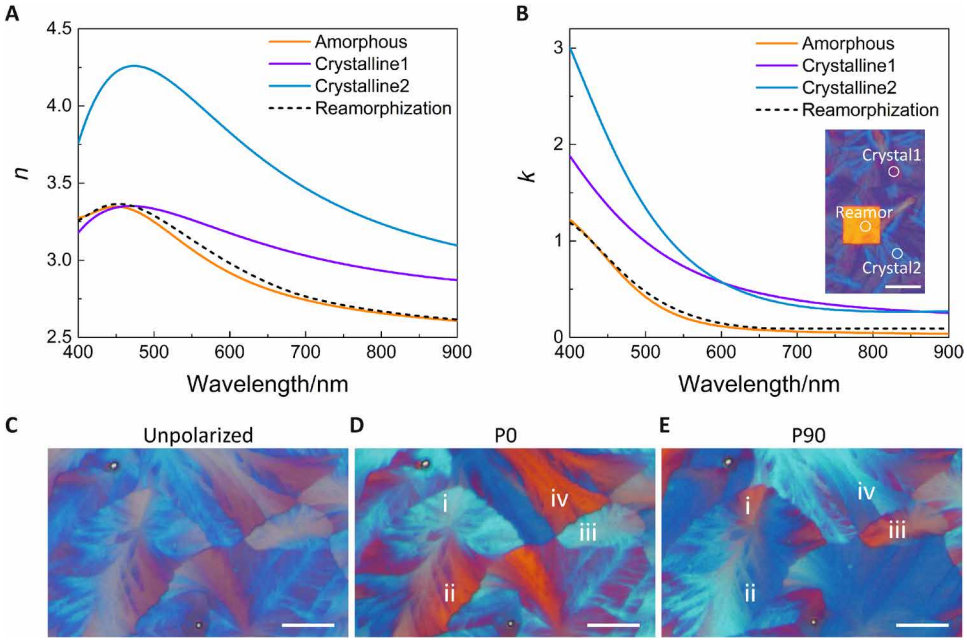

Fig. 3. Measured refractive indices of Sb_2S_3. (**A** and **B**) Measured refractive indices *n* and extinction coefficients *k* of 20-nm-thick Sb_2S_3 in the four-layer sample in amorphous, crystalline, and reamorphized states. Crystalline states 1 and 2 correspond to the birefringent orientations of the crystal grains seen as purple and blue, respectively, in Fig. 2A. Scale bar, 10 μm. (**C** to **E**) Optical micrographs of the anisotropic Sb_2S_3 crystals under unpolarized and mutually perpendicular polarizations. The crystals at areas (i) and (iii) appear blue under P0 and shift to purple color under P90. The opposite is true for areas (ii) and (iv). The two bright particles are used as the markers for positioning. Scale bars, 5 μm.

(ii)] is expected. Therefore, we measured the *n* and *k* dispersions for both in-plane anisotropies, as shown by the corresponding blue and purple lines in Fig. 3 (A and B). The crystalline optical constants for orientations of the crystal were higher than those measured for the amorphous state. Specifically, the refractive index of the extraordinary crystalline state (blue line) increased by a maximum of 1.0 across the entire visible range, which is larger than that of most widely studied typical PCMs, e.g., GST (see fig. S3) (*11*, *13*), Sb_2Te_3 (*34*), and $Ag_3In_4Sb_{76}Te_{17}$ (AIST) (*12*). We also compared the measured optical constants of the completely reamorphized square area with the as-deposited amorphous Sb_2S_3 film. Notably, the optical constants of the reamorphized Sb_2S_3 are close to that of the as-deposited amorphous film, as shown by the short dashed lines in Fig. 3 (A and B). To verify that the color change in Fig. 2A (ii) is due to the refractive index change afforded by phase transition (instead of thickness variation), we simulated the reflectance spectra and their corresponding colors of the sample in Fig. 2A (i and ii). The results shown in fig. S4 are in good agreement with the experimental data, indicating that the refractive index change induced by phase transition had led to the color changes in the device.

Notably, the birefringence of Sb_2S_3 crystals contributes to the colors of the crystalline film. We investigate the colors of the anisotropic crystals under mutually perpendicular polarizations, as shown in Fig. 3 (C to E). Each crystal displays interchangeable colors under mutually perpendicular polarizations, i.e., either blue or purple. These birefringent Sb_2S_3 crystals could be used to control light in polarization-dependent photonic waveguide devices. Moreover, we simulated the angle dependence of the reflected color using the measured refractive indices, as shown in fig. S5. The reflectance spectra are insensitive to the angles of incidence between 0° and 50°. As the angle was increased to 70°, the resonance noticeably blue-shifts, and the reflected color lightens because of the increase in Fresnel reflectance. This viewing angle insensitivity is typical for ultrathin and weakly absorbing films on metallic reflectors.

In addition to phase transitions, the thickness of the Sb_2S_3 film also influences the color of the rewritable device. We investigated the color dependence on the thickness of Sb_2S_3 films in both amorphous and crystalline states, as shown in Fig. 4. Figure 4A shows the measured colors of the rewritable device with varying Sb_2S_3 thickness from 10 to 70 nm. A range of amorphous-state colors including yellow, orange, brown, cyan, and pink were observed. After thermal annealing at 300°C for 2 min, the corresponding crystalline state of the samples appears inhomogeneous (because of birefringence) and exhibits a change in color.

To quantify the distributions of these amorphous and crystalline colors, we plotted them on the CIE (International Commission on Illumination) chromaticity diagram, as shown in Fig. 4D. The color difference between amorphous and crystalline states is substantial. Moreover, both the amorphous and crystalline devices occupy a substantial gamut within the sRGB (standard Red Green and Blue) color space. Reflectance spectra were measured to underpin this color difference, as shown in Fig. 4C. Notably, the first cavity mode spans from 400 to 750 nm with increasing thickness of Sb_2S_3 from 10 to 50 nm. The resonance dips of the structure can also be explained using the multilayer thin-film model (see fig. S6). Increasing Sb_2S_3 thickness beyond ~50 nm shifts the first-order resonance into the near-infrared region and the second cavity mode into the visible region. The FWHM of second-order mode is narrower than that of the first-order mode, and therefore, the amorphous colors with thickness larger than 50 nm are more saturated. Matching simulations

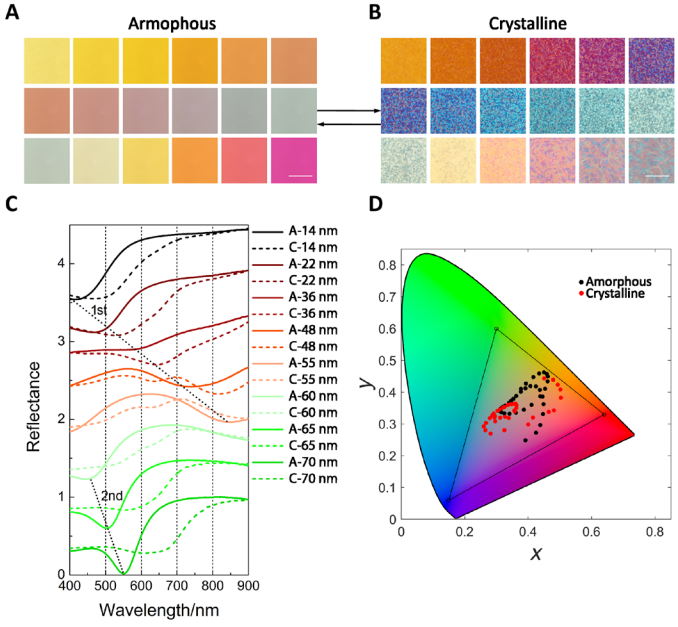

Fig. 4. Color palettes of the rewritable devices in amorphous and crystalline states for different thicknesses of Sb_2S_3. (**A** and **B**) Amorphous (left) and crystalline (right) color palettes with Sb_2S_3 thickness varying from 10 to 70 nm. Scale bars, 100 μm. (**C**) Reflectance spectra from representative color patches. Solid lines represent the amorphous state, and short dashed lines represent the crystalline state. With increasing thickness of Sb_2S_3, the fundamental (first resonance dip, as indicated) red-shifts out into the infrared and the second harmonic resonance appears within the visible spectrum. (**D**) Color coordinates from measured spectra plotted on the CIE 1931 chromaticity diagram of the devices with the thickness of the Sb_2S_3 film varying from 10 to 70 nm.

of these results are shown in fig. S7. The discrepancy between the simulated and experimental crystalline colors arises from the averaging of the refractive indices of crystalline states 1 and 2 (Crystalline1 and Crystalline2 in Fig. 3A). Overall, the simulations are in good agreement with the experimental results. We can thus realize a wider gamut of colors by varying both the thickness and crystalline/amorphous states of Sb_2S_3.

To compare the achievable range of colors of Sb_2S_3 with the prototypical PCMs, i.e., GST, GeTe (*34*, *35*), and AIST (*12*), we substituted the optical constants of Sb_2S_3 with those of other PCMs and calculated their color coordinates, as shown in fig. S8. Notably, the device incorporating Sb_2S_3 exhibits the widest color gamut by a notable margin. The large refractive index change (maximum $\Delta n > 1$) and the relatively small absorption effect (k) in the visible region are responsible for the wider color gamut of Sb_2S_3. In contrast, the large absorption effects (extinction coefficient, k) of GST, GeTe, and AIST limit their color range (specifically in the crystalline state), rendering them less suitable for photonic devices in the visible spectrum.

Superresolution printing

To investigate the feasibility of subdiffraction resolution printing, we performed laser exposure tests in pulse (discrete dots) and "continuous" (lines) modes. The pulse mode involved exposing an array of dots on the PCM device one point at a time, while the lines are continuously deflected by the laser beam in continuous mode. For both cases, the exposure time for each dot was 0.02 ms (corresponding to ~1600 pulses).

Figure 5 (A and B) shows the test results under pulse mode on the four-layer sample with 20- and 15-nm crystalline Sb_2S_3, respectively, in which we have written a series of dot arrays for a range of periodicities (d) ranging from 1.4 to 0.6 μm. To show the ability to resolve the dots, we selected four neighboring dots along the x axis from the samples with d = 0.6, 0.7, 1.0, and 1.4 μm in Fig. 5B and measured their color intensities, as shown in Fig. 5D. We can see from the color intensity that each pair of neighboring dots can be resolved with FWHM of the dots measuring ~560 nm. Notably, the center-to-center distance of the dots was smaller than the theoretical resolving power of our laser [$d = \lambda/2NA = 780/(2 \times 0.5) = 780$ nm] focused by a 20× objective with numerical aperture (NA) = 0.5. In addition, the device with a thinner layer of Sb_2S_3 (Fig. 5B) achieved a slightly higher resolution than the thicker layer (Fig. 5A), as less energy was needed to induce the phase transition (10.0 mW for 15 nm and 12.0 mW for 20 nm). Some dots in the arrays with smaller pitches, e.g., p = 0.8 μm in the 20-nm film, exhibit a larger positional variation than those in the device with 15-nm-thick Sb_2S_3. A possible reason could be related to the crystal size of Sb_2S_3. Large sizes of crystals in the 20-nm film lead to larger edges or boundaries among neighboring crystals, resulting in more distorted dots.

To test the resolution of continuous lines, we patterned lines with varying pitch in the 15-nm-thick Sb_2S_3 film, as shown in Fig. 5C. The grating lines patterned at a pitch of 0.6 μm can still be resolved. Overall, subdiffraction resolution was achieved in both pulse and continuous modes.

We calculated the internal heat distributions of the device by using a two-temperature model (*36*) to explore the underlying physics that enables subdiffraction printing resolution, as shown in Fig. 5 (E and F). The simulation details are provided in the Supplementary Materials. Although a two-photon lithography (TPL) system was used for the patterning, calculations show that single-photon absorption at 780 nm in Sb_2S_3 was sufficient to account for the heating. Figure 5 (E and F) shows in-plane and cross-sectional views of the temperature distribution in the center of Sb_2S_3. It is clear that the heat is contained within the Sb_2S_3 layer, and the lattice temperature in the center is higher than the melting temperature (*37*), which is required for melt-quench reamorphization (550°C). The diameter of the heated area with a temperature greater than that of the reamorphized spot is ~600 nm. Therefore, the crystalline device can be switched back to the amorphous state with a subdiffraction resolution, in agreement with experimental results. The subdiffraction-limited patterning is thus achievable because of the nonlinear thermal response of the material, i.e., near the threshold temperature for melting. This effect is consistent with other subwavelength laser writing effects in PCMs. Notably, two-photon absorption processes are orders of magnitude weaker than single-photon linear absorption, and our calculations show that single-photon absorption accounts for the necessary temperature rise for reamorphization.

From a design consideration, having a 3-nm-thick top layer of Al will increase the overall color brightness and gamut (*18*) but, unfortunately, will not work well with the 780-nm femtosecond laser, which was used in this work for amorphization. In the presence of the Al film, field localization and heating occur within the first two layers (i.e., top Al and Si_3N_4, as shown in fig. S9B) instead of the Sb_2S_3 layer, as shown in Fig. 5F (reproduced in fig. S9A). The laser pulses thus easily damage the Al films. As shown in fig. S9, only a small part of Sb_2S_3 is heated above its melting point, while the temperature of the top Al layer almost reaches the melting point of bulk Al. As a result,

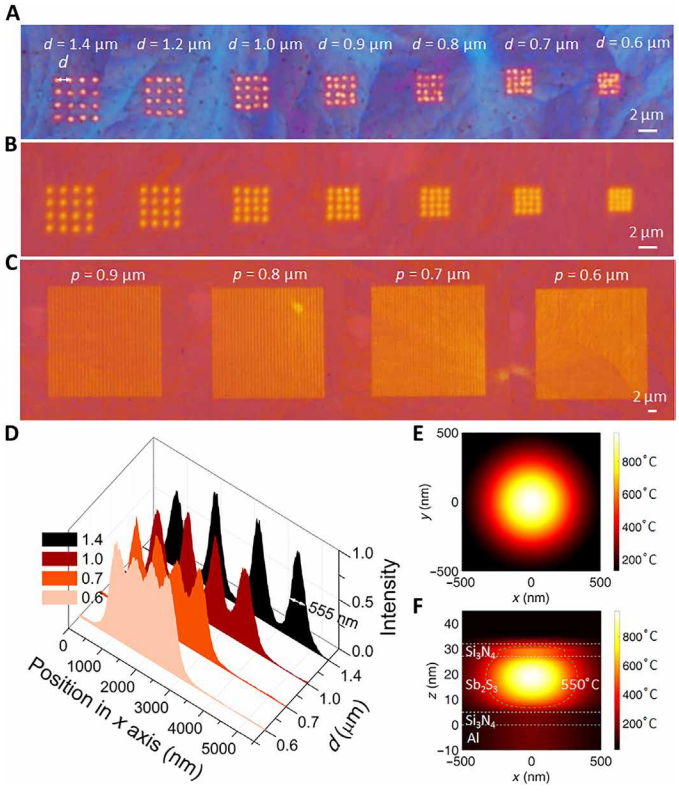

Fig. 5. Superresolution printing via laser switching of PCM. (**A**) Optical micrograph of resolution test dot arrays in 20-nm-thick Sb_2S_3 in pulse mode. Identical patterns written in 15-nm-thick Sb_2S_3 in pulse mode (**B**) and grating lines in continuous mode (**C**). Pitch (center-to-center distance) of neighboring dots and gratings are marked as *p* and *d*, respectively. (**D**) Measured average color intensities of four neighboring dots in the *x* direction with *d* = 0.6, 0.7, 1.0, and 1.4 μm in (A) (intensities normalized). Calculated temperature distribution within the *xy* plane of Sb_2S_3 layer (**E**) and cross section (**F**) of the device.

the top Al layer will be easily damaged with only a small part of Sb_2S_3 switching back to its amorphous state. We used the same setup to reamorphize the structures with a top Al film, as shown in fig. S9 (C to F). A small increase of the laser energy beyond a level that is close to full switching will damage the structure. Therefore, the presented structure (without a top Al film) is more appropriate for rewriteable optical devices.

Rewritable color prints

Having shown that the states of Sb_2S_3 can be repeatedly switched between crystalline, amorphous, and intermediate states, we now use this effect and the corresponding color change to realize rewritable color printing. The principle process of rewritable chalcogenide color printing is as follows: First, a crystalline four-layer ($Si_3N_4/Sb_2S_3/Si_3N_4$/Al) device with a fixed thickness of Sb_2S_3 is selected as the sample to be written. Second, a color image or print is written onto the sample by switching each crystalline pixel to amorphous or an intermediate state according to the designed pixel colors. Colors were adjusted by varying the laser power for each pixel. Third, the written image or print is erased by switching the amorphous or intermediate states back to the crystalline state by thermal annealing on a hot plate. By repeating steps 2 and 3, new images or prints can be rewritten onto the same area of the sample multiple times.

Figure 6A shows optical micrographs of our rewritable color prints. First, we selected the crystalline sample with a 20-nm-thick Sb_2S_3 layer as the rewritable device, which has a blue/purple background in crystalline state and yellow/orange color in amorphous state. We patterned the self-portrait of Vincent van Gogh in the TPL system. The color printing results are shown in Fig. 6A (i). By tuning the laser power at each exposure point, different colors were realized by partially or completely reamorphizing the crystalline Sb_2S_3 sample. Figure 6A (ii) shows the effect of thermal annealing the sample at 300°C for 2 min on a hot plate. The image was erased, thus making it possible to write a new image in the same area. The slight change in color of the erased region indicates the area where previous prints were made. We then patterned another Vincent van Gogh painting, *Vase with Fourteen Sunflowers*, in the same area, as shown in Fig. 6A (iii). Subsequently, we erased the painting of the *Vase with Fourteen Sunflowers* and patterned a different Vincent van Gogh's self-portrait on the same area at a smaller size, as shown in Fig. 6A (iv). Figure S10 shows a zoomed-out image of the color prints relative to a scratch mark that assisted the positioning of these color prints on the same area. Although Sb_2S_3 consist of anisotropic crystals (blue and purple), we applied the same laser power to switch them back to the amorphous state and did not consider the damage threshold for each crystal orientation. Hence, orientations that require less energy to reamorphize exhibit some degradation, as shown in fig. S10. In addition, because of the birefringence patterns in the Sb_2S_3 crystals, we investigated the polarization dependence of our color prints, as shown in fig. S10D. Notably, the background crystalline colors are polarization dependent and switchable, while the reamorphized areas are polarization independent.

Different thicknesses of Sb_2S_3 provide options for the color tones of rewritable paintings. Figure 6B shows the optical microscopy images of the three states of the sample with a 15-nm-thick layer of Sb_2S_3. With increasing laser powers from 2.0 to 10.0 mW, crystalline regions were gradually switched back to the amorphous state. The power levels are ~20% lower than those required to switch the thicker 20-nm films. Figure 6C shows the rewritable results on this sample in a similar manner with the thicker films. First, we printed the *Girl with a Pearl Earring* on a crystalline sample with 15-nm-thick Sb_2S_3 (Fig. 6C, i), performed an erase step (Fig. 6C, ii), and finally printed over the same area the painting of *Mona Lisa*, as shown in Fig. 6C (iii). The pixel size in the TPL printing was set at 500 nm by 500 nm, corresponding to a print resolution of ~4.35×10^4 dpi.

DISCUSSION

We demonstrate a solid-state, ultrathin, super-high-resolution, and rapid-switching programmable color printing device that exploits large refractive index changes induced by structural transitions in Sb_2S_3. By gradually tuning the average laser power of femtosecond laser pulses, an intermediate partially crystalline state forms as evidenced by Raman spectroscopy, reflectance resonances, and measured optical constants. With the help of femtosecond laser pulses and a thermal anneal, the interference colors can be cycled back and forth by tuning the structural states of the chalcogenide material. Furthermore, we printed and erased different color images in the same area of the device with subdiffraction resolutions. Wider color gamut and active visible photonic devices can be realized by incorporating Sb_2S_3 in the feed gap of gap-plasmon cavities or directly used as nanoantennas in dielectric metamaterials. Specifically, we believe that this is the first report of a

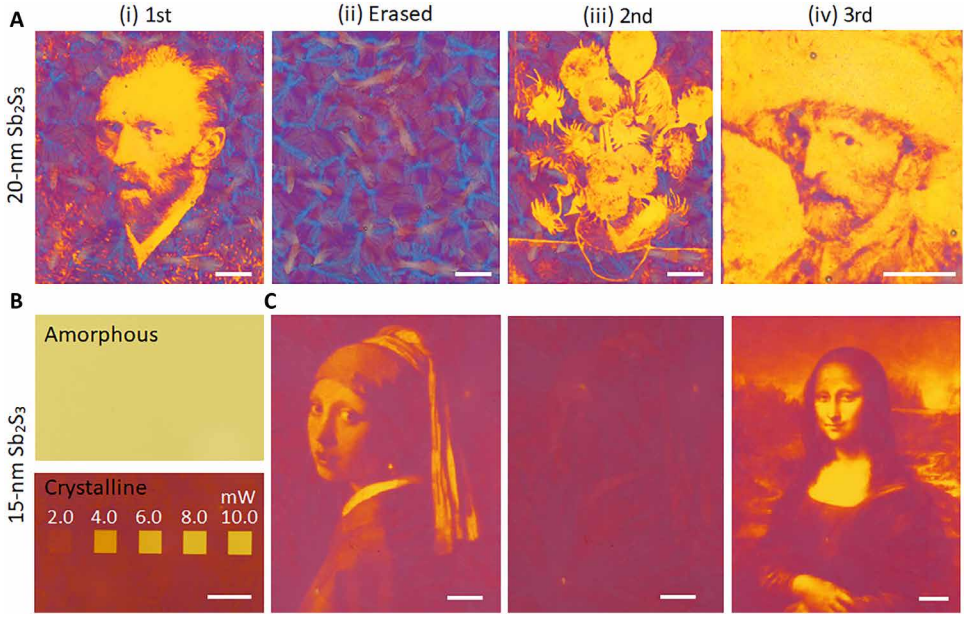

Fig. 6. Rewritable chalcogenide color microprints. (**A**) Optical micrographs of the same region of sample with 20-nm-thick Sb_2S_3 showing (i) the self-portrait painting of Vincent van Gogh, (ii) the erased sample in crystalline state after thermal annealing, (iii) a print of the *Vase with Fourteen Sunflowers* of Vincent van Gogh as the second image patterned on the same area, and (iv) a second self-portrait painting of Vincent van Gogh written as the third image after erasing the sample a second time. (**B**) Optical microscopy images of the amorphous, crystalline, and the reamorphized color patches of the sample with 15-nm-thick Sb_2S_3. The color patches with laser power from 2.0 to 8.0 mW correspond to intermediate states. The color patch with power of 10.0 mW is switched back to amorphous state. (**C**) Rewritable color prints on the same area of the sample with 15-nm-thick Sb_2S_3. Micrograph of *Girl with a Pearl Earring* (Johannes Vermeer, 1665) written as the first color print (left). Erased sample with thermal annealing (middle). *Mona Lisa* (Leonardo da Vinci) written as the second painting on the same area (right). Scale bars, 20 μm.

birefringent PCM that can be amorphized with femtosecond pulse trains at high repetition rate and subdiffraction-limited patterns. Usually, one needs fast cooling or quenching to amorphize PCMs, but here, we demonstrate that it is possible to amorphize with 80-MHz cycles of femtosecond pulse trains, which suggests that any cumulative heating effect is small. We believe that this is likely due to the subdiffraction-limited volume of Sb_2S_3, which is heated by the laser. Because the heated volume is small, negligible heat is trapped within the structure and fast quenching is possible within the 12.5-ns cycle between the femtosecond pulses. We expect that the proposed ultrathin and subdiffraction rewritable color printing method and the previously unknown characteristics of Sb_2S_3 are useful for next-generation high-resolution color display devices and optical encryption.

MATERIALS AND METHODS

Materials

The aluminum film was first deposited on Si (001) substrate using an electron beam evaporator (Kurt J. Lesker Company) at a pressure of 1.1×10^{-6} torr, and then, $Si_3N_4/Sb_2S_3/Si_3N_4$ were sequentially deposited with radio frequency sputtering under a base pressure of 3×10^{-7} torr. Sb_2S_3 was deposited from a pure Sb_2S_3 target in an argon (Ar) atmosphere with a flow of 10 sccm (standard cubic centimeters per minute), and the Si_3N_4 was deposited from a pure Si target in an Ar:N_2 = 8:2 (8-sccm Ar and 2-sccm N_2) reactive mixture. The sputtering pressure was 3.7 mtorr (~0.5 Pa), and the working distance was 140 mm. The crystalline samples were achieved with heating the amorphous samples on a hot plate at 300°C for 2 min.

Color image printing

The predesigned images were first coded with MATLAB and Describe programming languages, and each pixel of the images was transferred to a matrix including the position and power information of the laser pulses. We use the femtosecond laser pulses generated from the commercial direct laser printing system (Nanoscribe Inc., Germany) to reamorphize the crystalline sample and to write the color images in Fig. 6. The wavelength of the femtosecond laser is 780 nm, and the repetition rate and pulse width are 80 MHz and 100 fs, respectively. The output power of the laser can be controlled with an accuracy of 0.1 mW.

Reflectance and Raman measurement

Reflectance spectra were measured with a Nikon Eclipse LV100ND optical microscope equipped with a microspectrophotometer (CRAIC), and the optical microscopy images were taken with a Nikon DS-Ri2 camera. Raman spectra were collected with a WITec alpha300 system equipped with a 532-nm laser.

Refractive index measurement

The refractive indices of amorphous, crystalline, and intermediate states of Sb_2S_3 were measured with an imaging ellipsometer (nanofilm_ep4, Accurion GmbH). Anisotropy refractive indices were achieved with an attachment for Mueller matrix measuring. All the refractive indices were measured under a 20× microscope objective.

Numerical calculations

The simulated reflectance spectra and the corresponding color patches of simulations in figs. S1, S4, S7, and S8 are calculated with

the commercial FDTD software (Lumerical Solutions). The heat distributions in Fig. 4 are calculated with the finite element method software COMSOL Multiphysics. An electromagnetic two-temperature model is built on the basis of the non-equilibrium thermal process to simulate the femtosecond laser pulse interaction with our designed system (details are provided in the Supplementary Materials).

SUPPLEMENTARY MATERIALS

Supplementary material for this article is available at http://advances.sciencemag.org/cgi/content/full/6/51/eabb7171/DC1

REFERENCES AND NOTES

1. X. Zhu, C. Vannahme, E. Højlund-Nielsen, N. A. Mortensen, A. Kristensen, Plasmonic colour laser printing. *Nat. Nanotechnol.* **11**, 325–329 (2016).
2. K. Kumar, H. Duan, R. S. Hegde, S. C. W. Koh, J. N. Wei, J. K. W. Yang, Printing colour at the optical diffraction limit. *Nat. Nanotechnol.* **7**, 557–561 (2012).
3. Y. Jin, I. Qamar, M. Wessely, A. Adhikari, K. Bulovic, P. Punpongsanon, S. Mueller, Photo-chromeleon: Re-programmable multi-color textures using photochromic dyes, in *Proceedings of the 32nd Annual ACM Symposium on User Interface Software and Technology* (ACM, 2019), pp. 701–712.
4. S. J. Tan, L. Zhang, D. Zhu, X. M. Goh, Y. M. Wang, K. Kumar, C.-W. Qiu, J. K. W. Yang, Plasmonic color palettes for photorealistic printing with aluminum nanostructures. *Nano Lett.* **14**, 4023–4029 (2014).
5. H. Liu, J. Xu, H. Wang, Y. Liu, Q. Ruan, Y. Wu, X. Liu, J. K. W. Yang, Tunable resonator-upconverted emission (TRUE) color printing and applications in optical security. *Adv. Mater.* **31**, 1807900 (2019).
6. Z. Dong, J. Ho, Y. F. Yu, Y. H. Fu, R. Paniagua-Dominguez, S. Wang, A. I. Kuznetsov, J. K. W. Yang, Printing beyond sRGB color gamut by mimicking silicon nanostructures in free-space. *Nano Lett.* **17**, 7620–7628 (2017).
7. Y. Liu, H. Wang, J. Ho, R. C. Ng, R. J. H. Ng, V. H. Hall-Chen, E. H. H. Koay, Z. Dong, H. Liu, C.-W. Qiu, J. R. Greer, J. K. W. Yang, Structural color three-dimensional printing by shrinking photonic crystals. *Nat. Commun.* **10**, 4340 (2019).
8. H. Kim, J. Ge, J. Kim, S.-e. Choi, H. Lee, H. Lee, W. Park, Y. Yin, S. Kwon, Structural colour printing using a magnetically tunable and lithographically fixable photonic crystal. *Nat. Photonics* **3**, 534–540 (2009).
9. M. A. Kats, R. Blanchard, P. Genevet, F. Capasso, Nanometre optical coatings based on strong interference effects in highly absorbing media. *Nat. Mater.* **12**, 20–24 (2013).
10. Y. M. Andreeva, V. C. Luong, D. S. Lutoshina, O. S. Medvedev, V. Y. Mikhailovskii, M. K. Moskvin, G. V. Odintsova, V. V. Romanov, N. N. Shchedrina, V. P. Veiko, Laser coloration of metals in visual art and design. *Opt. Mater. Express* **9**, 1310–1319 (2019).
11. P. Hosseini, C. D. Wright, H. Bhaskaran, An optoelectronic framework enabled by low-dimensional phase-change films. *Nature* **511**, 206–211 (2014).
12. C. Ríos, P. Hosseini, R. A. Taylor, H. Bhaskaran, Color depth modulation and resolution in phase-change material nanodisplays. *Adv. Mater.* **28**, 4720–4726 (2016).
13. H.-K. Ji, H. Tong, H. Qian, N. Liu, M. Xu, X.-S. Miao, Color printing enabled by phase change materials on paper substrate. *AIP Adv.* **7**, 125024 (2017).
14. S. Yoo, T. Gwon, T. Eom, S. Kim, C. S. Hwang, Multicolor changeable optical coating by adopting multiple layers of ultrathin phase change material film. *ACS Photonics* **3**, 1265–1270 (2016).
15. R. E. Simpson, P. Fons, A. V. Kolobov, T. Fukaya, M. Krbal, T. Yagi, J. Tominaga, Interfacial phase-change memory. *Nat. Nanotechnol.* **6**, 501–505 (2011).
16. K. Chaudhary, M. Tamagnone, X. Yin, C. M. Spägele, S. L. Oscurato, J. Li, C. Persch, R. Li, N. A. Rubin, L. A. Jauregui, K. Watanabe, T. Taniguchi, P. Kim, M. Wuttig, J. H. Edgar, A. Ambrosio, F. Capasso, Polariton nanophotonics using phase-change materials. *Nat. Commun.* **10**, 4487 (2019).
17. Q. Wang, E. T. F. Rogers, B. Gholipour, C.-M. Wang, G. Yuan, J. Teng, N. I. Zheludev, Optically reconfigurable metasurfaces and photonic devices based on phase change materials. *Nat. Photonics* **10**, 60–65 (2016).
18. W. Dong, H. Liu, J. K. Behera, L. Lu, R. J. H. Ng, K. V. Sreekanth, X. Zhou, J. K. W. Yang, R. E. Simpson, Wide bandgap phase change material tuned visible photonics. *Adv. Funct. Mater.* **29**, 1806181 (2019).
19. L. Shao, X. Zhuo, J. Wang, Advanced plasmonic materials for dynamic color display. *Adv. Mater.* **30**, 1704338 (2018).
20. D. Franklin, Y. Chen, A. Vazquez-Guardado, S. Modak, J. Boroumand, D. Xu, S.-T. Wu, D. Chanda, Polarization-independent actively tunable colour generation on imprinted plasmonic surfaces. *Nat. Commun.* **6**, 7337 (2015).
21. H. You, A. Steckl, Three-color electrowetting display device for electronic paper. *Appl. Phys. Lett.* **97**, 023514 (2010).
22. S. Shang, Q. Zhang, H. Wang, Y. Li, Fabrication of magnetic field induced structural colored films with tunable colors and its application on security materials. *J. Colloid Interf. Sci.* **485**, 18–24 (2017).
23. H. Cho, S. Han, J. Kwon, J. Jung, H.-J. Kim, H. Kim, H. Eom, S. Hong, S. H. Ko, Self-assembled stretchable photonic crystal for a tunable color filter. *Opt. Lett.* **43**, 3501–3504 (2018).
24. X. Duan, S. Kamin, N. Liu, Dynamic plasmonic colour display. *Nat. Commun.* **8**, 14606 (2017).
25. M. Huang, A. J. Tan, F. Büttner, H. Liu, Q. Ruan, W. Hu, C. Mazzoli, S. Wilkins, C. Duan, J. K. W. Yang, G. S. D. Beach, Voltage-gated optics and plasmonics enabled by solid-state proton pumping. *Nat. Commun.* **10**, 5030 (2019).
26. G. J. Stec, A. Lauchner, Y. Cui, P. Nordlander, N. J. Halas, Multicolor electrochromic devices based on molecular plasmonics. *ACS Nano* **11**, 3254–3261 (2017).
27. W. Wang, N. Xie, L. He, Y. Yin, Photocatalytic colour switching of redox dyes for ink-free light-printable rewritable paper. *Nat. Commun.* **5**, 5459 (2014).
28. X. Zhu, W. Yan, U. Levy, N. A. Mortensen, A. Kristensen, Resonant laser printing of structural colors on high-index dielectric metasurfaces. *Sci. Adv.* **3**, e1602487 (2017).
29. J.-M. Guay, A. C. Lesina, G. Côté, M. Charron, D. Poitras, L. Ramunno, P. Berini, A. Weck, Laser-induced plasmonic colours on metals. *Nat. Commun.* **8**, 16095 (2017).
30. A. S. Roberts, S. M. Novikov, Y. Yang, Y. Chen, S. B. Boroviks, J. Beermann, N. A. Mortensen, S. I. Bozhevolnyi, Laser writing of bright colors on near-percolation plasmonic reflector arrays. *ACS Nano* **13**, 71–77 (2019).
31. F.-Z. Shu, F.-F. Yu, R.-W. Peng, Y.-Y. Zhu, B. Xiong, R.-H. Fan, Z.-H. Wang, Y. Liu, M. Wang, Dynamic plasmonic color generation based on phase transition of vanadium dioxide. *Adv. Opt. Mater.* **6**, 1700939 (2018).
32. I. Efthimiopoulos, C. Buchan, Y. Wang, Structural properties of Sb_2S_3 under pressure: Evidence of an electronic topological transition. *Sci. Rep.* **6**, 24246 (2016).
33. R. G. A. Garcia, C. A. M. Avendaño, M. Pal, F. P. Delgado, N. R. Mathews, Antimony sulfide (Sb_2S_3) thin films by pulse electrodeposition: Effect of thermal treatment on structural, optical and electrical properties. *Mater. Sci. Semicond. Proc.* **44**, 91–100 (2016).
34. H.-K. Ji, H. Tong, H. Qian, Y.-J. Hui, N. Liu, P. Yan, X.-S. Miao, Non-binary colour modulation for display device based on phase change materials. *Sci. Rep.* **6**, 39206 (2016).
35. S. G.-C. Carrillo, L. Trimby, Y.-Y. Au, V. K. Nagareddy, G. Rodriguez-Hernandez, P. Hosseini, C. Ríos, H. Bhaskaran, C. D. Wright, A nonvolatile phase-change metamaterial color display. *Adv. Opt. Mater.* **7**, 1801782 (2019).
36. E. L. Gurevich, Y. Levy, S. V. Gurevich, N. M. Bulgakova, Role of the temperature dynamics in formation of nanopatterns upon single femtosecond laser pulses on gold. *Phys. Rev. B* **95**, 054305 (2017).
37. Ž. Živković, N. Štrbac, D. Živković, D. Grujičić, B. Boyanov, Kinetics and mechanism of Sb_2S_3 oxidation process. *Thermochim. Acta* **383**, 137–143 (2002).
38. M. Hu, G. V. Hartland, Heat dissipation for Au particles in aqueous solution: Relaxation time versus size. *J. Phys. Chem. B* **106**, 7029–7033 (2002).
39. A. O. Govorov, H. H. Richardson, Generating heat with metal nanoparticles. *Nano Today* **2**, 30–38 (2007).
40. T. B. Nasr, H. Maghraoui-Meherzi, N. Kamoun-Turki, First-principles study of electronic, thermoelectric and thermal properties of Sb_2S_3. *J. Alloy. Compd.* **663**, 123–127 (2016).

Acknowledgments: We would like to thank D. Matthias, P. Thiesen, and F. Sebastian in Accurion GmbH for help in measuring the microscale refractive index of Sb_2S_3. **Funding:** This research is supported by National Research Foundation (NRF) Singapore, under its Competitive Research Programme (CRP15-2015-03) and the SUTD Digital Manufacturing and Design (DManD) Center (grant RGDM 1830303). R.E.S. acknowledges the NLSM project (grant A18A7b0058) with A*STAR. **Author contributions:** H.L., W.D., J.K.W.Y., and R.E.S. conceived the idea. W.D., L.L., and R.E.S. fabricated the materials. H.L. did the experiments, characterizations, and simulations. Q.R., H.L., and Y.S.T. simulated the reflectance spectra. H.W. finished the simulations for thermal heat distributions. H.L., J.K.W.Y., and R.E.S. drafted the manuscript. All the authors discussed the results and commented on the manuscript. **Competing interests:** The authors declare that they have no competing interests. **Data and materials availability:** All data needed to evaluate the conclusions in the paper are present in the paper and/or the Supplementary Materials. Additional data related to this paper may be requested from the authors.

Submitted 13 March 2020
Accepted 27 October 2020
Published 16 December 2020
10.1126/sciadv.abb7171

Citation: H. Liu, W. Dong, H. Wang, L. Lu, Q. Ruan, Y. S. Tan, R. E. Simpson, J. K. W. Yang, Rewritable color nanoprints in antimony trisulfide films. *Sci. Adv.* **6**, eabb7171 (2020).